Research on Engineering Structures & Materials
www.jresm.org

Research Article

Dynamic behavior of high damping rubber bearings and lead rubber bearings under near-fault earthquakes

Dhirendra Patel[*,a], Rajesh Kumar[b] , Vishal Kumar Mourya[c], Gaurav Pandey[d]

Department of Civil Engineering, Indian Institute of Technology-BHU, Varanasi, India

Article Info

Article history:

Received 25 Feb 2024
Accepted 05 Apr 2024

Keywords:

Base isolation;
High damping rubber bearing;
Lead rubber bearing;
ABAQUS;
Earthquakes

Abstract

Civil engineering structures are susceptible to natural calamities such as earthquakes, floods, and strong winds. Base isolation is a proven method for protecting structures during earthquakes. It involves inserting a flexible layer between the foundation and superstructure to isolate the structure from earthquakes, thereby changing the system's dynamic characteristics. The present study compares the dynamic performance of passive base isolators, specifically High Damping Rubber Bearings (HDRBs) and Lead Rubber Bearings (LRBs), under near-fault ground motion conditions to assess their effectiveness in reducing seismic impact on structures. The isolator is first analyzed using a static general approach and validated against existing literature before undergoing dynamic analysis. In this research, the LRB isolation system is analyzed using a dynamic explicit approach in ABAQUS, while the HDRB is analyzed using a dynamic implicit approach. The behavior of these isolators is studied under seismic events such as those from the Imperial Valley, Managua, Loma Prieta, Northridge, and Kocaeli ground motions. The results indicate that LRBs significantly reduce acceleration at the top of the bearing compared to HDRBs. The maximum reductions in response are 68.42% for the Kocaeli earthquake in case of LRBs and 61.80% for the Northridge earthquake in case of HDRBs. The LRB shows a minimum acceleration response reduction of 57.24%, while for HDRB, it is 24.47% for the Imperial Valley records in both cases.

1. Introduction

Earthquakes are ancient, unpredictable hazards that disrupt the ground, affecting structures and systems, often with significant consequences. Structural designers and engineers face a challenge in mitigating these effects. Extensive research has led to strategies to strengthen structures against seismic forces. This vulnerability is often observed in existing buildings where some storeys lack walls, making them susceptible to larger earthquake forces and increased lateral deformations. Worldwide, buildings collapse during earthquakes, requiring costly retrofitting to extend their service life [1].

Seismic hazard in regions is determined by geological, tectonic, and statistical data. Key parameters include earthquake epicenter, hypocenter, duration, source parameters, and intensities. Earthquakes are crucial for testing structural behavior under horizontal loads [2]. Studies conducted in the Balkan countries and neighboring regions, like Turkey and Iran, have experienced destructive earthquakes in recent years, causing significant damage and even building collapse [3]. Post-disaster studies are essential for assessing earthquake hazards, understanding factors affecting building performance, and guiding urban

[*]Corresponding author: dhirendrapatel.rs.civ17@itbhu.ac.in
[a] orcid.org/0009-0004-1633-2437; [b] orcid.org/0000-0001-5145-588x; [c] orcid.org/0009-0009-4348-9911; [d] orcid.org/0009-0008-3750-3097
DOI: http://dx.doi.org/10.17515/resm2024.194ea0225rs

planning and structural design [4]. Furthermore, a study was conducted to examined seismic damage to masonry buildings, focusing on low and mid-rise masonry residential buildings in Albania constructed between 1940 and 1990 under pre-modern seismic codes. The study aims to compare their seismic behavior under near-field and far-field earthquake scenarios [5].

Base isolation employs specially designed devices between the superstructure and foundation to isolate the structure from seismic motion as shown in Fig. 1 [6-8]. Seismic isolation is a technique aimed at diminishing inertial forces generated within a structure during earthquake ground shaking. It achieves a shift in the fundamental period of vibration by uncoupling the superstructure from the supporting foundation through the use of isolators, elements that are laterally flexible yet vertically stiff [9]. Decoupling involves extending a building's natural vibration period, reducing spectral acceleration (Fig. 2). This shift in the structural time-period, depicted in Fig. 3, results in greater relative displacements [10]. Seismic Base Isolation (BI) is an innovative, globally adopted approach in earthquake-resistant design.

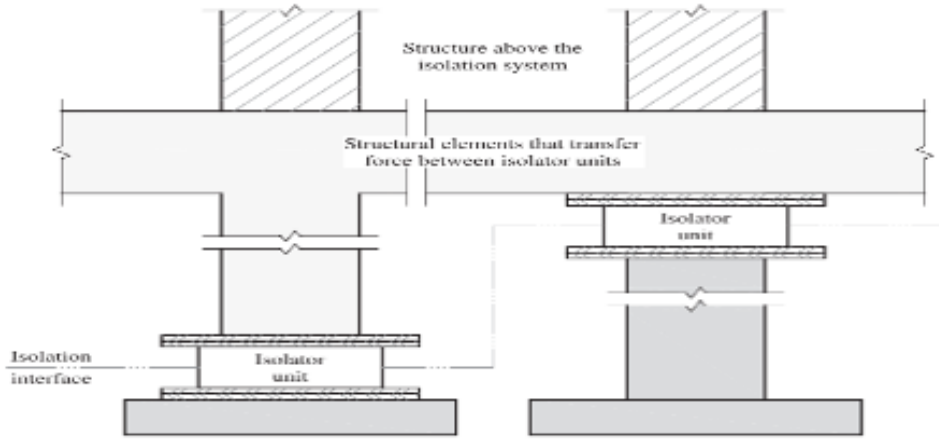

Fig. 1. Base Isolation terminology (ASCE 7-16)

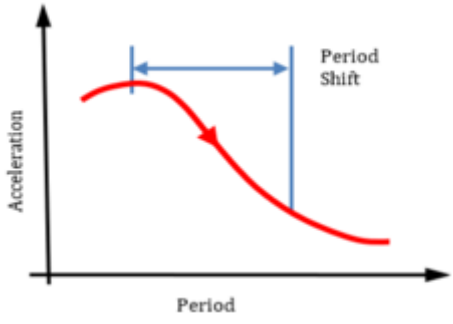

Fig. 2. Time period shift

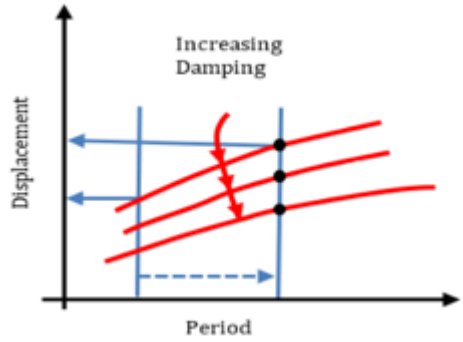

Fig. 3. Displacement design response spectra

The two primary techniques for earthquake resistance in structures are conventional earthquake-resistant design and seismic isolation. Conventional methods strengthen structures with features like shear walls or braced frames but can lead to issues like excessive floor acceleration or inter-story drifts. Seismic isolation, especially base

isolation, is increasingly popular for protecting structures in earthquake-prone areas from intense ground motion [11].

The rubber material is derived from Hevea brasiliensis latex, natural rubber, initially known as "Caoutchouc," was termed "rubber" by Joseph Priestley in 1770. Fisher introduced "elastomer" in 1939 for synthetic rubber-like materials. Charles Goodyear's 1839 vulcanization discovery and DuPont's 1931 Neoprene creation revolutionized rubber properties. Fillers, accelerators, anti-ozonants, and antioxidants improve rubber compounds. Natural rubber pads absorbed impact in a Melbourne rail bridge in 1889. Eugene Freyssinet's 1954 patent paved the way for widely used multilayer rubber bearings in earthquake-resistant designs [12]. In 1981, Robinson integrated lead cores into rubber bearings, resulting in the creation of Lead Rubber Bearings (LRBs), aimed at improving energy dissipation [13]. The HDRB is exemplified by the 1985 Foothill Communities Law and Justice Center, offer high stiffness and damping at low shear strains and increased resilience under major earthquakes. Modeling HDRB behavior in seismic design considers factors like creep, rate dependence, mechanical properties, manufacturing variations, and environmental influences [14].

HDRBs are characterized by their ability to provide high stiffness and damping at small shear strains, effectively reducing their behavior to service and wind loads. They also exhibit low shear stiffness but with suitable damping capability at the design displacement level. As displacement amplitudes intensified, HDRBs show a notable increase in stiffness and damping, which is beneficial in restraining movements during major ground motions [12]. When modeling HDRB behavior in seismic isolation systems, it is essential to consider various factors. Creep, a significant consideration, makes the response of these devices rate reliable. Additionally, mechanical features can be affected by manufacturing variations, contact pressure, loading and strain history, temperature fluctuations, and aging effects. HDRB along with low-damping natural rubber bearings and LRBs, are usually implemented as seismic base-isolation system [14]. The complex structure of HDRBs involves adding fine carbon blocks, oils, resins, and other fillers to natural rubber, enhancing their damping properties. This modification leads to non-linear hysteretic material behavior during earthquake loads, posing challenges in accurately representing their actual performance [15]. Laminated elastomeric bearings, featuring rubber and steel layers bonded through vulcanization, are widely used. The inclusion of steel shim layers enhances vertical stiffness with minimal impact on shear stiffness. However, excessive damping at smaller displacements may affect the system's overall effectiveness and internal equipment [10]. The study analyzed two adjacent three-story buildings in India's highest seismic zone: one on a Lead Rubber Bearing (LRB) base isolator and the other a conventional RC framed structure. Real earthquake responses from 2006 to 2007 were recorded. The LRB building had a frequency 2.6 times lower than the conventional one, with a response reduction of 4 to 5 times. Structure-soil-structure interaction was observed in the LRB building's response, aligning with the nearby structure's frequency. Numerical simulations and soil modeling validated the results. During a larger earthquake with a PGA of 0.26 g, the LRB building's response acceleration was about 4.1 times lower than the conventional structures [16]. Furthermore, the effect of soil-structure interaction is studied [17-19].

The choice of a suitable material model and the determination of its parameters significantly impact the accuracy and reliability of finite element analysis results for rubber components like tires, engine mounts, and rubber bearings. Typically, two types of mechanical models are employed for rubber materials: hyper-elastic and hyper-viscoelastic models. The former is suitable for simpler problems where time effects can be disregarded, while the latter is essential for analyses involving time-dependent factors, such as dissipated energy determination in cyclic loading (hysteresis). Despite extensive

research on hyper-elastic models, hyper-viscoelastic models have received less attention, and further work is needed to document and determine their parameters adequately.

The study was conducted to evaluates seismic-isolated bridges using LRBs under near-field earthquake with discrete pulse responses. It examines maximum isolator displacements (MIDs) and maximum isolator forces (MIFs), accounting for LRB yield strength deterioration due to heating. The comparison includes deteriorating and non-deteriorating conditions, employing bounding analyses. Nonlinear response history analyses, considering different soil conditions, reveal that lower bound analyses tend to overestimate MIDs, especially for LRBs with higher Q/W ratios, during near-field earthquakes with increased velocity pulses [20]. The paper also investigates the impact of lead core heating on LRB-isolated bridges under near-field ground motions, validating bounding analyses for designing maximum isolator force and displacement envelopes. Results indicate that temperature rise in the lead core correlates with higher magnitudes and more near-fault earthquakes pulses, decreasing with greater distances from the fault. [21]. Earthquake excitations were applied to a 20-story RC and a 3-story steel structure to investigate the impact of isolator characteristics, including isolation period and characteristic strength-to-weight ratio, on the behaviour of the superstructures [22]. LRB base-isolated buildings, designed with optimal yield strength ratios, demonstrate robust seismic performance, even in mega earthquake scenarios, surpassing structures using critical yield strength and second shape coefficients [23]. Rubber material parameters are derived from laboratory tests, including uniaxial tensile and relaxation tests. The 3D-FE model of the bearing is then compared with an analytical ABAQUS CAE model for LRB isolators, showing good agreement in shear behaviour [24]. The inclusion of a lead core in a lead rubber bearing (LRB) improves its performance by enabling energy dissipation, enhancing damping characteristics, increasing vertical stiffness, and ensuring overall reliability. The lead core is engineered to plastically deform under lateral loads, effectively absorbing substantial energy during seismic events and minimizing force transmission to the structure. This deformation isolates the structure from ground motion, reducing the likelihood of structural damage. Furthermore, the lead core boosts the bearing's vertical stiffness, supporting the structure and ensuring stability under varying loads.

RRB (rubber bearing with steel rings) is implemented in 3 to 6-story steel and concrete building, compared to fixed and isolated base structures with LRB. Abaqus is used for finite element modelling, showing average effective stiffness of 110.88 (ton/m) for LRB and 82.48 (ton/m) for RRB, with damping at 18.44% for LRB and 47.02% for RRB. Nonlinear time history analysis with earthquake records reveals RRB isolated base structures achieve reductions in acceleration by 42.16%, 43.36%, 51.83%, and 57.16% for 3, 4, 5, and 6-story buildings. Shear reductions are 55.5%, 47.16%, 37.93%, and 56.83%, and drift decreases are 35.33%, 50%, 54.5%, and 59.66% for 3, 4, 5, and 6-story structures [25]. The research refines the estimation of yield strength and confinement of lead cores in Lead Rubber Bearings (LRB). Prototype tests reveal variability, challenging the traditional use of a standard lead yield value (7-10 MPa). The study validates a newly developed equation for estimating yield strength based on lead core confinement. Comparisons with prototype tests demonstrate a good match, with differences mostly within ±5% [26]. The value-based seismic design framework to optimize the geometrical and mechanical characteristics of LRBs has been studied. Considering construction cost and seismic consequences as key components, the optimization problem accounts for multiple LRB failure modes, such as strength weakening, axial buckling, and rubber rupture [27]. The study assesses the influence of LRB and HDRB on structures using nonlinear finite element analyses with SAP 2000. Isolator designs follow the UBC code [28]. This research presents a novel approach for designing base-isolated buildings in line with Algerian seismic regulations. The method combines the linear equivalent approach for design displacement using an iterative

process with time history analysis. Numerical modelling, compared with global regulations, validates the approach, demonstrating satisfactory results in design displacement and base shear force alignment [29]. The study was conducted to investigate the impact of pulse-like ground motions on seismically isolated buildings using three near-fault record sets with varying pulse periods. Two seismically isolated RC buildings were designed following ASCE-7-16 standards. Each records spectrum was scaled to the Risk-Targeted Maximum Considered Earthquake level spectrum using the amplitude scaled approach in the scaling period range of ASCE 7–16. The buildings were then subjected bidirectionally to the scaled records. Results for two different scaling period ranges were compared to assess their effects on isolator displacements [30]. Moreover, a 40-story building subjected to near-fault and far-field strong motion records were examined. Results compared various factors such as story drift ratios, wall shear stresses, and beam rotations. It is common to reduce shear wall thickness at upper levels, but this study found that doing so can lead to early elastic capacity in the core-wall, altering post-yield shear force redistribution below the yielding level [31]. The study was conducted to developed fragility curve for five building by using FEMA P695. It found a strong link between isolation unit collapse probability and the isolation system displacement ratio. Simple, highly correlated equations were developed to estimate required displacement capacity for specific risk-target levels. These equations were validated against two building models and compared with IDA results, showing their applicability for the preliminary design of mid-rise isolated reinforced concrete buildings [32].

This study employs Abaqus CAE 2020 software to validate the static analysis of the LRB model with existing experimental and numerical analysis. Subsequently, the LRB and HDRBs are analyzed for dynamic response, comparing acceleration responses at the base and top of the loading plate under ground motion inputs. For dynamic analysis, five near-fault earthquakes are selected from PEER NGA West2 records. Despite extensive research on various isolation systems, including LRBs and HDRBs, there is a notable scarcity of studies examining the dynamic performance in relation to their mechanical characteristics and material properties. This study investigates the impact of seismic isolators, specifically HDRBs and LRBs, on key seismic parameters. The uniqueness of the work lies in its comparative analysis of these base isolators under various seismic events, providing valuable insights for isolator design. A micro modelling of the isolator is performed using finite element modelling software ABAQUS, and both LRBs and HDRBs are subjected to different near-fault ground motions to gain insights into their dynamic response. The results are compared with the input earthquake values, and the response reduction is presented as a percentage decrease in acceleration response. Additionally, the time-displacement response is provided for the Imperial Valley and Managua earthquake records.

2. Theory and Design of LRB and HDRB for Finite Element Dynamic Analysis

A FEM holds the potential to serve as a robust tool for advancing our understanding of the local behavior of seismic isolation devices. Kelly applied FE modeling to investigate the variation in lateral force-displacement response under increasing axial load, employing a 2-D model [33]. Imbimbo and Luca [34] conducted FE analyses on circular elastomeric bearings subjected to vertical loads. Doudoumis [35] employed numerical modeling, utilizing finite element micromodels, for Lead-Rubber Bearings, revealing enhanced possibilities for a detailed study of stress, strain, and available strength. Despite these advancements, there has been a lack of comprehensive comparison between theoretical and numerical models for laminated rubber bearings in previous finite element modeling efforts. This research addresses this gap by first detailing the process of 3-D FE analysis modeling for a laminated rubber bearing. Subsequently, through a comparison of the FE

analysis outcomes with experimental findings, the validity of the models is demonstrated. The analysis procedure for the current study is depicted in the Fig. 4.

3. Material Properties, Dimensions and Loading Condition

When selecting numerical models for LRBs and HDRBs in Abaqus, prioritize accuracy, reliability, and compatibility. The materials for models must be chosen that accurately represent hyper elastic rubber and lead behavior under dynamic loading, ensuring they can perform dynamic analysis and simulate contact with surrounding structures accurately. The models must be validated against experimental data, consider computational efficiency for numerical simulation in Abaqus.

Fig. 4. The flow chart illustrates the analysis procedure of the present study

The LRB used in this study is the Skellerup150 isolator, which is listed in the Skellerup Industries manufacturer's catalogue [36]. The inclusion of steel in rubber isolators is crucial for mitigating excessive strains under vertical loads and is commonly represented as an elastoplastic material. Steel's properties include a yield stress of 240 MPa, a Poisson's ratio of 0.3, and an elastic modulus of 210 GPa. Lead, with a crystal structure undergoing alterations with increasing displacement, is characterized by a yield stress of 19.5 MPa, a Poisson's ratio of 0.43, and a modulus of elasticity of 18000 MPa. The assembly comprises two top and bottom loading steel plates, each with a diameter of 601 mm and a thickness

of 31.8 mm. Additionally, there are two fixing steel plates (top and bottom) with a diameter of 431 mm and a thickness of 25.4 mm. The configuration includes 11 rubber layers, each with a diameter of 431 mm and a thickness of 9 .5 mm, as well as 10 steel shims measuring 431 mm in diameter and 3.0 mm in thickness. At the core is a central lead core with a diameter of 116.8 mm and a height of 185 mm. According to the specifications, the design compressive load is 667 kN, and the lateral design displacement is 0.1524 m [35].

Before moving to dynamic analysis, a preliminary static analysis is performed to optimize the dimensions of the bearing. The analysis of the LRB is conducted using ABAQUS CAE (User's Manual V6.14). Initially, the model is subjected to vertical static loadings. After applying a vertical compressive load of 667 kN, a cyclic horizontal displacement with an amplitude of ±1524 mm is applied, based on the specified dimensions. The analysis includes analytical results from numerical simulations conducted in Abaqus. A comparison is made with the force-displacement curves provided by the manufacturer and Doudoumins 2005, illustrated in Fig. 5.

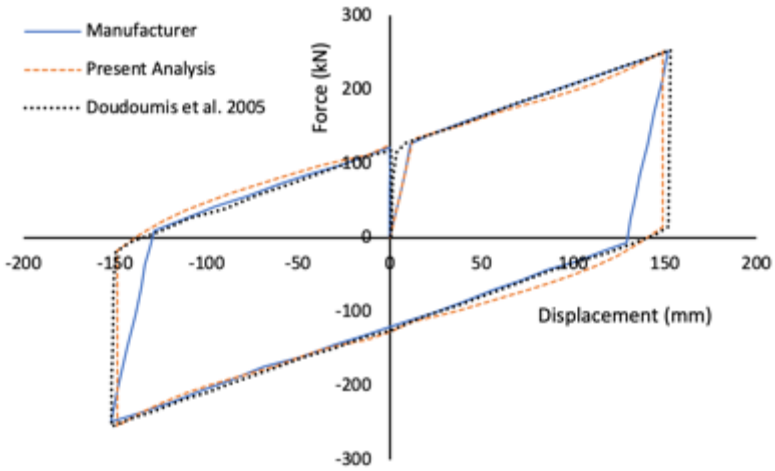

Fig. 5. Comparison of the force-displacement curves obtained from analytical (Abaqus), experimental and Doudoumis et al. results

3.1 Selecting a Rubber Constitutive Model for Dynamic Analysis

Rubber is identified as an incompressible material, retaining a constant volume during deformations, which classifies it as isochoric. In rubber compounds, volume alterations are minimal, nearing incompressibility. This results in a Poisson's ratio of 0.5, constraining the use of classical computational mechanics for stress and strain calculations. The elastic characteristics of rubber in terms of potential strain energy function U in terms of Green's deviatoric strain invariants are as follows:

$$U = f(I_1, I_2, I_3) \tag{1}$$

I_1, I_2, I_3 are first, second and third deviatoric strain invariant of the green deformation tensor in terms of $\lambda_1, \lambda_2, \lambda_3$.

$$I_1 = \lambda_1^2 + \lambda_2^2 + \lambda_3^2 \tag{2}$$

$$I_2 = \lambda_1^2\lambda_2^2 + \lambda_2^2\lambda_3^2 + \lambda_3^2\lambda_1^2 \tag{3}$$

$$I_3 = \lambda_1^2\lambda_2^2\lambda_3^2 \tag{4}$$

The rubber's hyper-elasticity is characterized by the Yeoh model, and its damping response is modeled using the Prony series viscosity model. A comprehensive overview of both the Yeoh hyper-elasticity model and the Prony series viscosity model is available in the accompanying Table1 and Table 2.

3.1.1 Yeoh Model

The strain energy function for the Yeoh model

$$U = C_{10}(\bar{I}_1 - 3) + C_{20}(\bar{I}_1 - 3)^2 + C_{30}(\bar{I}_1 - 3)^3 + \frac{1}{D_1}(J^{el} - 1)^2 + \frac{1}{D_2}(J^{el} - 1)^4 + \frac{1}{D_3}(J^{el} - 1)^6 \tag{5}$$

For N=3, the equation can be written as:

$$U = \sum_{i=1}^{3} C_{10}(\bar{I}_1 - 3)^i + \sum_{i=1}^{3} \frac{1}{D_i}(J^{el} - 1)^{2i} \tag{6}$$

C_{i0}, D_i are material constants, N= material constant (positive numbers N=1,2,3), μ, λ_m and D, are temperature-dependent parameters $D = \frac{2}{K}$; and $\bar{I}_1 = \bar{\lambda}_1^2 + \bar{\lambda}_2^2 + \bar{\lambda}_3^2$ and $\bar{I}_2 = \bar{\lambda}_1^{(-2)} + \bar{\lambda}_2^{(-2)} + \bar{\lambda}_3^{(-2)}$, where $\bar{\lambda}_i = J^{-\frac{1}{3}}\lambda_i$; J= Jacobean determinant where $J = \lambda_1\lambda_2\lambda_3$, J^{el} is the elastic volume ratio, and K is the bulk modulus.

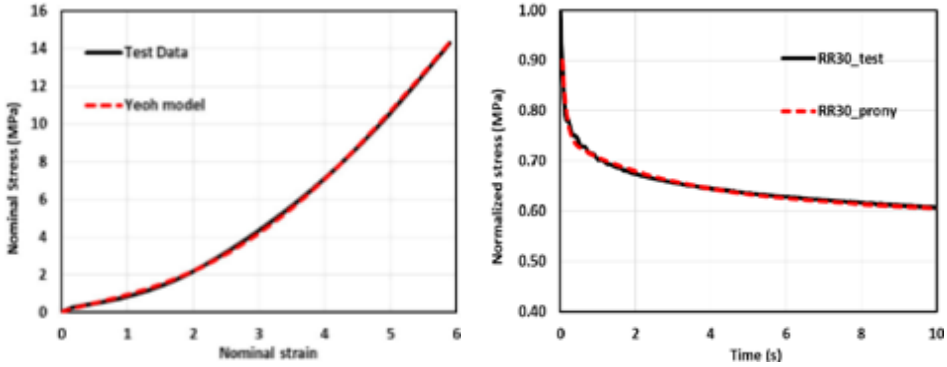

(a) (b)

Fig. 6. The uniaxial tensile test (a) results (black line) for the rubber specimen, along with the relaxation test results (b), are compared with their respective numerical models, represented by the red line

Table 1. Parameters for the Yeoh hyper-elasticity model applied to rubber material [24]

C_{10}	C_{20}	C_{30}
0.206	0.013	-0.000059

Table 2. Coefficients for the Prony series in rubber specimens [24]

i	G_i	t_i
1	0.25	0.103
2	0.11	2.664
3	0.08	26.06
4	0.25	924.24

The μ_i and α_i are constants which depend upon shear behaviour and D_i is compressibility. Fig. 6 displays the rubber specimen's strain-stress curve (black line), with Fig. 6(a) demonstrating alignment between test data and the Yeoh model. In Fig. 6(b), the relaxation data is compared with the Prony model [24].

4. Mechanical Parameters of LRB and HDRB

Total thickness of rubber

$$T_r = nt_r \tag{7}$$

where n is number of rubber layers, t_r is the thickness of the single rubber layer and T_r is total rubber layer thickness. Total height of the elastomeric rubber bearing;

$$h = nt_r + (n-1)t_s \tag{8}$$

where n is number of rubber layers, t_r is the thickness of the single rubber layer, t_s thickness of single layer steel shim and T_r is total rubber layer thickness. Bonded rubber area;

$$A = \frac{\pi}{4}[(D_0 + t_c)^2 - D_i^2] \tag{9}$$

Where, t_c is the rubber cover thickness, D_0 is the outer diameter and D_i is the inner thickness or lead core diameter (for LRB and for HDRB $D_i = 0$)

The zero-displacement force intercept (Q_d) in a LRB is determined by the shear yield strength of the lead (σ_L) and the area of cross-section for the lead plug (A_L). The characteristics strength for the bearing;

$$Q_d = \sigma_L A_L \tag{10}$$

The second-slope stiffness (K_d) refers to the elastomeric component stiffness of the bearing. At a specific horizontal displacement (d), the effective or secant stiffness of the LRB is given by:

$$K_{eff} = \frac{Q_d}{d} + K_d \tag{11}$$

Shape factor, is defined individually for a rubber layer as:

$$S = \frac{D_o - D_i}{4t_r} \tag{12}$$

The steel shims confine the rubber at the bond interface. The shim spacing (or thickness of rubber layer) regulates the bulging around the perimeter, influencing the compression modulus (E_c) of the elastomeric layer.

$$E_c = \left(\frac{1}{6GS^2F} + \frac{4}{3K_{bulk}}\right)^{-1} \tag{13}$$

Where, G is shear modulus, K_{bulk} is bulk modulus of rubber, S is shape factor, central hole factor $F = \frac{(r_d)^2+1}{(r_d-1)^2} + \frac{1+r_d}{(1-r_d)ln(r_d)}$, $r_d = \frac{D_o}{D_i}$

The tight arrangement of steel plates, or thin rubber layers, generates a substantial shape factor, leading to increased vertical stiffness.

$$K_v = \frac{AE_c}{T_r} \tag{14}$$

The overall rubber thickness (T_r) serves to offer the essential low horizontal stiffness required to extend the fundamental period of the system. Simultaneously, the tight arrangement of intermediate steel plates contributes substantial vertical stiffness and shear modulus is given as G and bonded rubber area (A). It's important to note that the steel shim plates do not influence the calculated horizontal stiffness of the bearing.

$$K_h = \frac{GA}{T_r} \tag{15}$$

Torsional Stiffness

$$K_t = \frac{2GI_s}{h} \tag{16}$$

Effective Period

$$T_{eff} = 2\pi\sqrt{\frac{W}{K_{eff}.g}} \tag{17}$$

Where, W is the seismic weight of the structure supported by the isolation unit g is gravitational acceleration.

Effective stiffness

$$K_{eff} = \frac{W}{g}\left(\frac{2\pi}{T}\right)^2 \tag{18}$$

Hysteresis loop defined the energy dissipation per cycle,

$$W_D = 2\pi K_{eff}\beta D^2 \tag{19}$$

The energy dissipated per loading cycle (E_{loop}) and the effective stiffness (K_{eff}) is determined based on the peak displacements, Δ^+ and Δ^-.

$$\beta_{eff} = \frac{2}{\pi}\frac{E_{loop}}{K_{eff}(|\Delta^+| + |\Delta^-|)^2} \tag{20}$$

Damping reduction factor

$$\frac{1}{B} = 0.25\left(1 - ln\beta_{eff}\right) \tag{21}$$

The design and construction of the isolation system must ensure resilience to, at the very least, the maximum displacement D ascertained through the upper and lower bound characteristics, particularly in the most critical horizontal response direction.

$$D = \frac{gS_aT_{eff}^2}{4\pi^2 B} \tag{22}$$

The force-deflection properties of an isolation system should be determined through cyclic load tests conducted on prototype isolation unit. For each loading cycle, the effective stiffness of the isolator, denoted as K_{eff}, must be calculated as per the specified

$$K_{eff} = \frac{|F^+| + |F^-|}{|\Delta^+| + |\Delta^-|} \tag{23}$$

Here, F^+ represents the positive force at the maximum positive displacement Δ^+, and F^- denotes the negative force at the minimum negative displacement Δ^- as shown in Fig. 7.

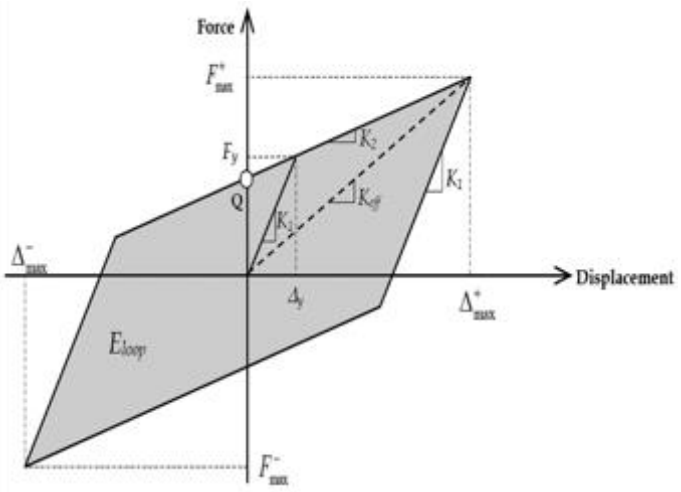

Fig. 7. Force-displacement hysteretic characteristic of an isolator (IS 1893 Part 6)

4.1. Modelling of HDRB for Dynamic Analysis

The HDRB was modeled in Abaqus CAE 2020 software, with its four parts (Loading Plate, Fixing Plate, Steel Plate, and Rubber Plate as shown in Fig. 8) created according to properties outlined in the 'Material Properties and Dimensions' section. The model was constructed in the Parts module, with material characteristics such as Poisson's coefficient, modulus of elasticity, density, and plastic properties, including visco-elastic coefficients and Yeoh model coefficients are defined. These properties were assigned to the respective sections, and the parts were assembled together.

To facilitate the dynamic analysis, two reference points are positioned at the centroids of the top and bottom surfaces of the model as shown in Fig. 9. The degrees of freedom for these surfaces are linked to their corresponding reference points. These reference points serve as anchors for applying boundary conditions and loading scenarios to the bearing. The simulation applied a general method with analysis procedure as Dynamic Implicit in the step module. The Interaction module in ABAQUS serves to define contact behaviors, such as friction or heat, between layers.

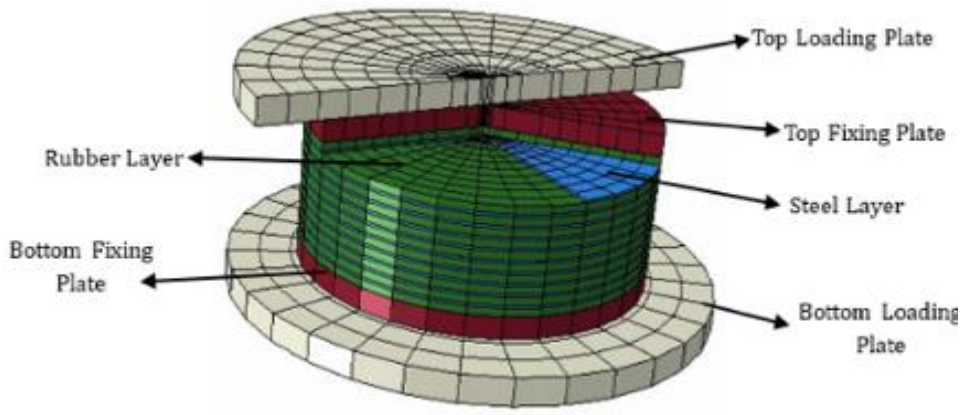

Fig. 8. Schematic representation of the HDRB with its components

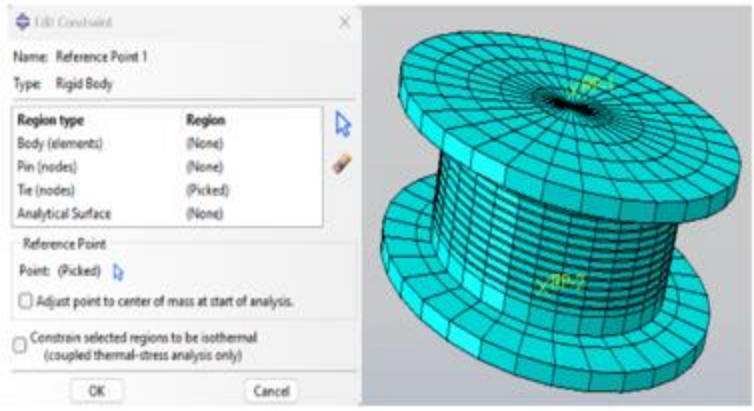

Fig. 9. Diagram depicts the reference point RP1 and RP2 at the top and bottom of the bearing

It also allows for the specification of how degrees of freedom are constrained and how parts are connected. In this study, the Tie constraint is utilized to attach the parts of the isolators, ensuring their cohesive movement as a single unit. The bearing was meshed to create 9222 elements. For the steel material, the C3D8R *Hex* element type (an 8-node linear brick with reduced integration and hourglass control) was selected, while for the visco-hyperelastic rubber material, the C3D20H *Hex* element type (a 20-node quadratic brick with hybrid linear pressure) was chosen. A concentrated force of 667kN was applied at the top of the loading plate of the bearing, and ground motion was applied at its bottom surface.

4.2. Modelling of Lead Rubber Bearing for Dynamic Analysis

The Lead Rubber Bearing was modelled in Abaqus CAE 2020 software, with its four parts (Loading Plate, Fixing Plate, Lead Core, Steel Plate, and Rubber Plate as shown in Fig. 10) created based on properties outlined in the 'Material Properties and Dimensions' section. The simulation used a general method with analysis procedure is used as Dynamic Explicit in the step module, employing Tie constraints to connect the parts.

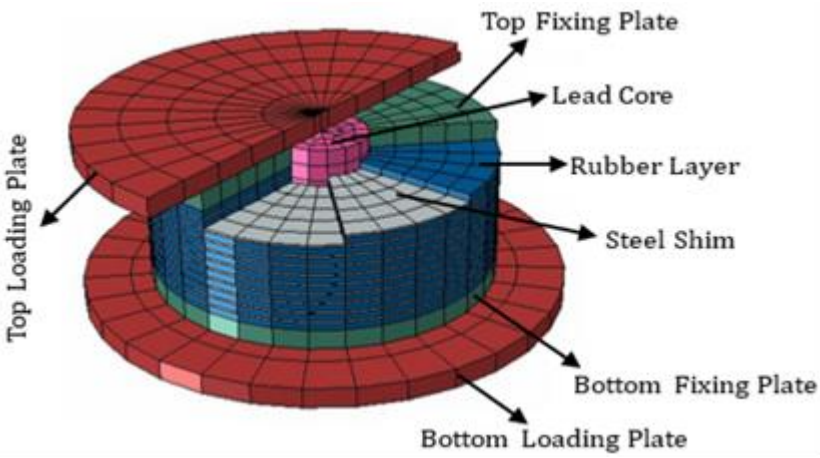

Fig. 10. Schematic representation of lead rubber bearing

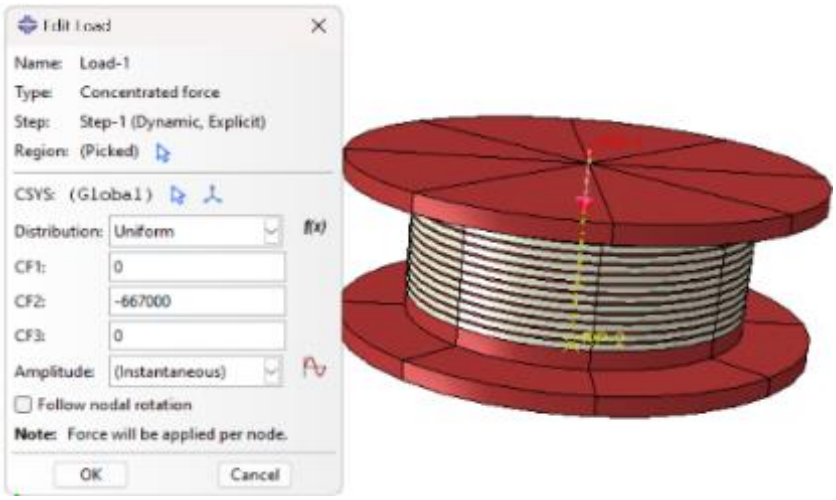

Fig. 11. Diagram depicts the applied concentrated load on LRB

The bearing was meshed with 4424 *Hex* elements, using the C3D8R element type (an 8-node linear brick with reduced integration and hourglass control). A concentrated force of 667kN was applied at the top of the loading plate of the bearing as shown in Fig. 11, and ground motion was applied at its bottom surface.

5. Properties of the Near-Fault Ground Motions

To examine the seismic performance of rubber bearings under earthquake excitations, five intense near-field ground motion records were chosen from the Pacific Earthquake Engineering Research Center [37], as listed in the Table 3. Near-fault ground motions are discerned by their long-period pulses and substantial ground displacements, which are notably greater than those observed in far-fault ground motions. Using the following earthquake specifications: Magnitude 7 > M_w > 6.0 and Distance (R) < 10 km, a search was conducted in the PEER NGA West2 Ground Motion Database. The input earthquake records are shown in Fig. 12 for Imperial Valley records and acceleration response spectra, Fig. 13 represents Managua record and acceleration response spectra, Fig. 14 represents Loma Prieta records and acceleration response spectra, Fig. 15 represents The Kocaeli records and acceleration response spectra and Fig. 16 represents Northridge records and acceleration response spectra. The Fourier Amplitude Spectrum for time history records is shown in Fig. 17.

Table 3. Properties of the applied near-fault ground motions Records

S. No.	Earthquake Record	Station Name	Year	Mechanism	RSN	Magnitude (M_w)	R_{jb} (km)	R_{rup} (km)	V_s30 (m/s)	PGA (g)	PGV (cm/s)	PGD (cm)
1.	Imperial Valley	El Centro Array #9	1940	Strike slip	6	6.95	6.09	6.09	213.4	0.233	31.29	18.44
2.	Managua, Nicaragua	Managua, ESSO	1972	Strike slip	95	6.24	3.51	4.06	288.7	0.354	28.41	6.096
3.	Loma Prieta	Saratoga,	1989	Reverse Oblique	802	6.93	7.58	8.5	380.8	0.369	47.32	26.53
4.	Northridge	Arleta Nordhoff	1994	Reverse	949	6.69	3.3	8.66	297.7	0.329	29.28	9.49
5.	The Kocaeli	Yarmica	1999	Strike Slip	1176	7.51	1.38	4.83	297	0.285	70.86	63.12

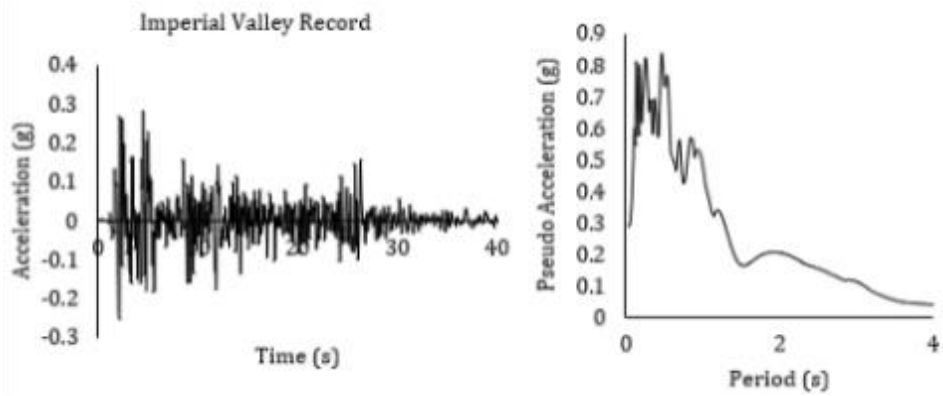

Fig. 12. Time histories recorded during the earthquake of Imperial Valley and Acceleration Response Spectra

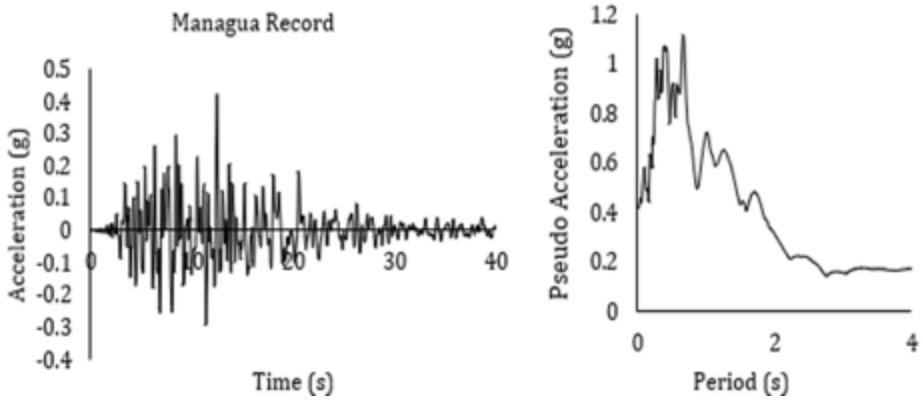

Fig. 13. Time histories recorded during the earthquake of Managua and Acceleration Response Spectra

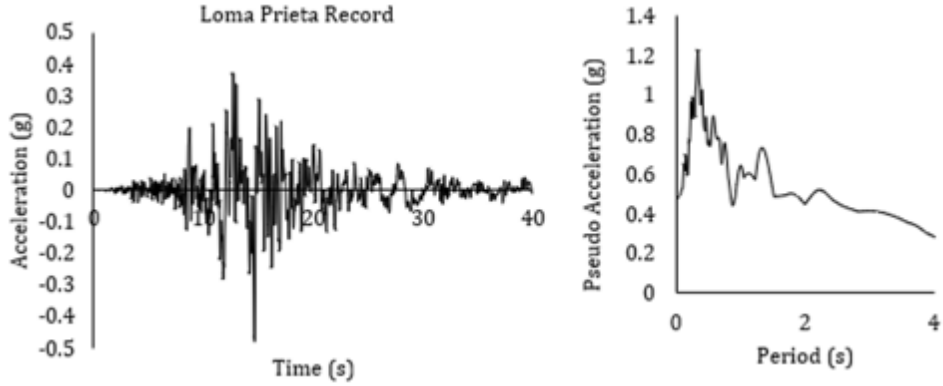

Fig. 14. Time histories recorded during the earthquake of Loma Prieta and Acceleration Response Spectra

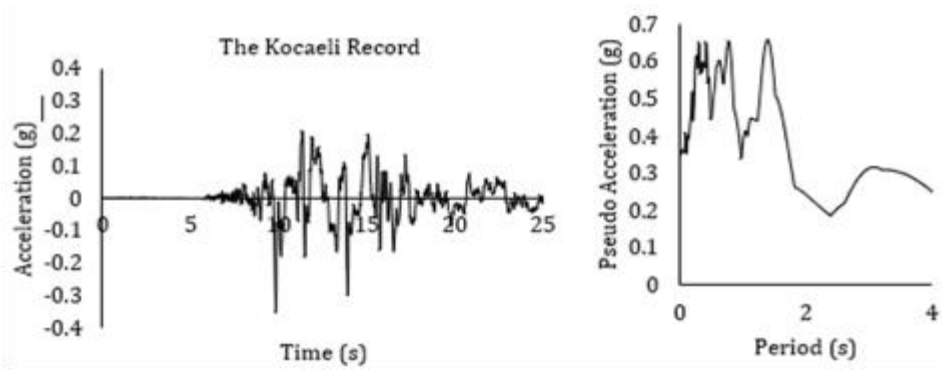

Fig. 15. Time histories recorded during the earthquake of The Kocaeli and Acceleration Response Spectra

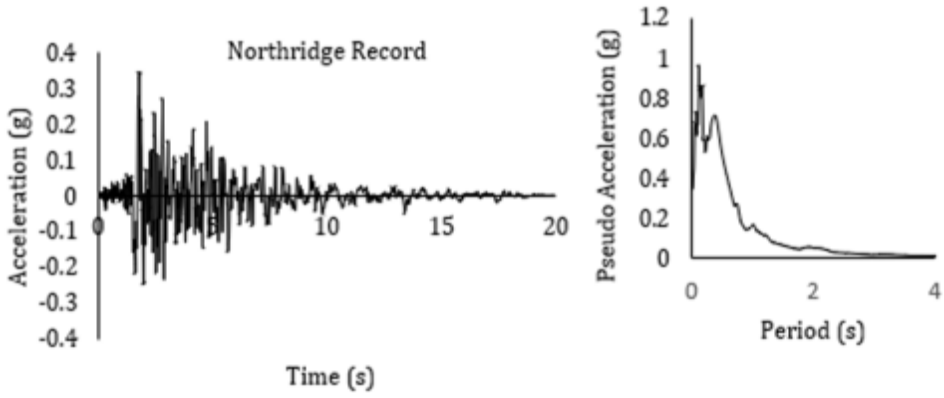

Fig. 16. Time histories recorded during the earthquake of Northridge and Acceleration Response Spectra

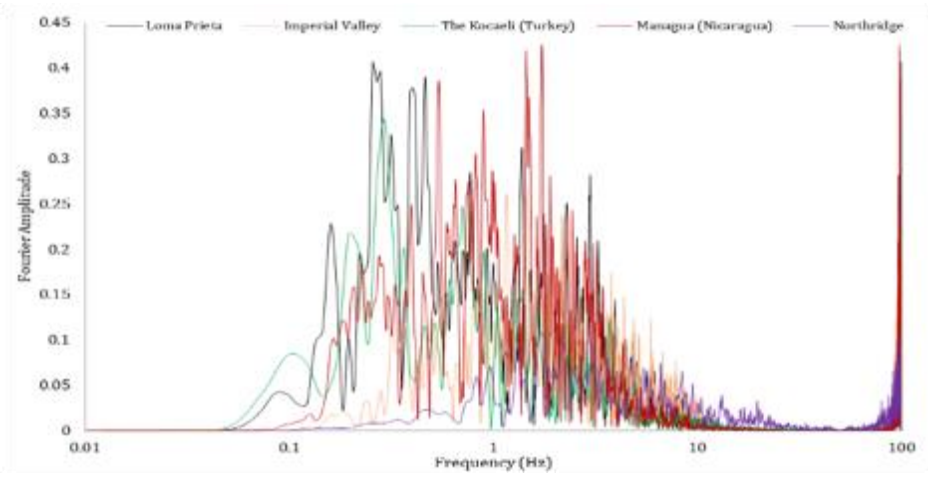

Fig. 17. Fourier amplitude spectrum of various time history records

6. Comparison of the Acceleration Response

The study examined the key features of the bearings and compared the input earthquakes reduced at the top of both LRBs and HDRBs. The inclusion of a lead core in the rubber bearing significantly decreased earthquake responses. The comparative results of Imperial Valley, Managua, Kocaeli, Northridge and Loma Prieta are shown in Fig. 18, Fig. 19, Fig. 20, Fig. 21 and Fig. 22, respectively. The bearings exhibited effective behavior during the input time history earthquakes, with maximum response reductions of 68.42% for the Kocaeli earthquake in the case of LRBs and 61.80% for the Northridge earthquake in the case of HDRBs.

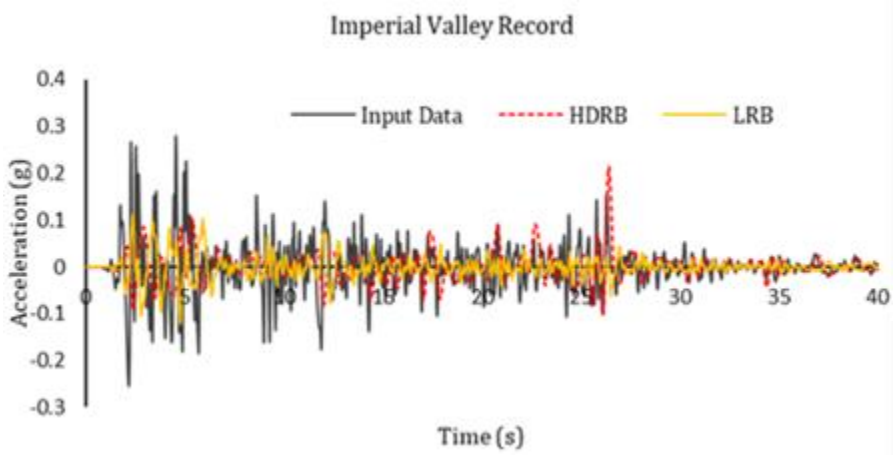

Fig. 18. Comparison of the Top bearing acceleration obtained from the dynamic analysis of the HDRB and LRB models under the input Imperial Valley earthquake

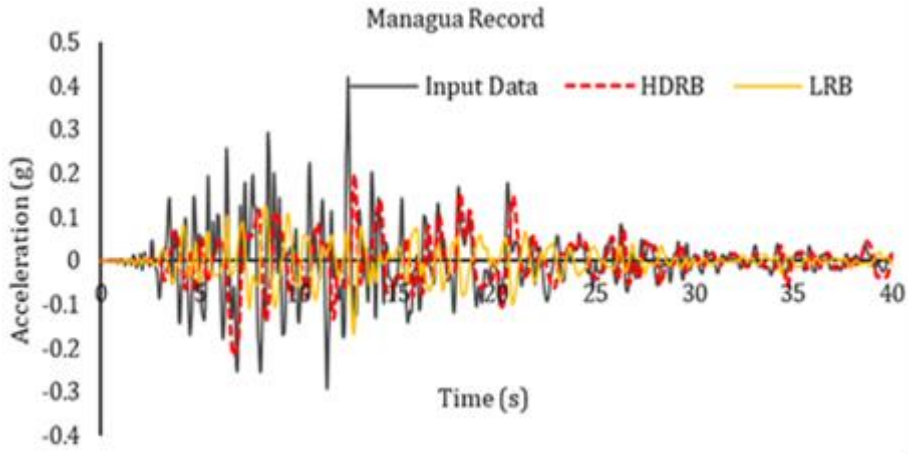

Fig. 19. Comparison of the Top bearing acceleration obtained from the dynamic analysis of the HDRB and LRB models under the input Managua earthquake

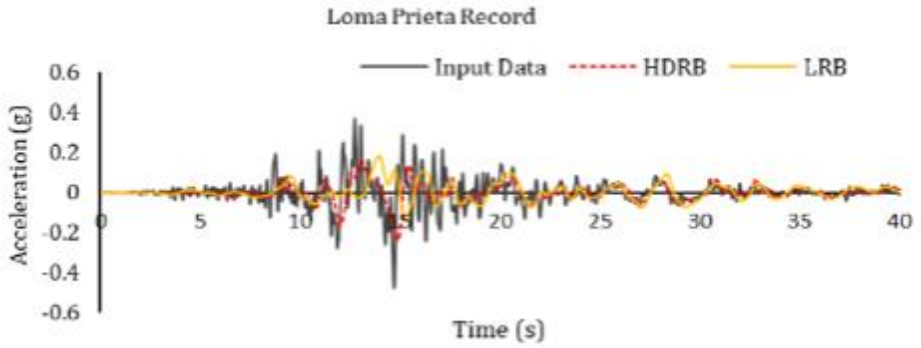

Fig. 20. Comparison of the Top bearing acceleration obtained from the dynamic analysis of the HDRB and LRB models under the input Loma Prieta earthquake

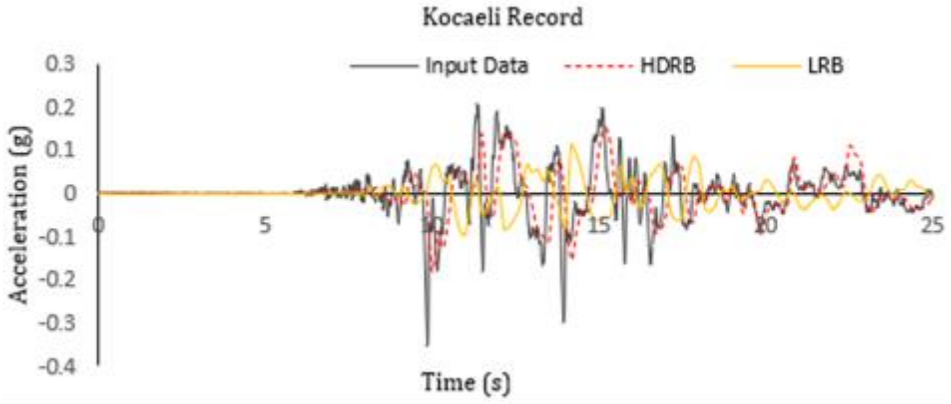

Fig. 21. Comparison of the Top bearing acceleration obtained from the dynamic analysis of the HDRB and LRB models under the input The Kocaeli earthquake

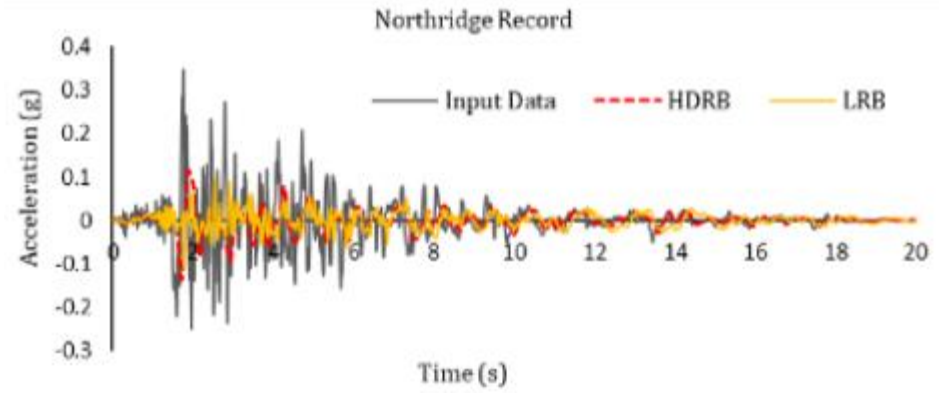

Fig. 22. Comparison of the Top bearing acceleration obtained from the dynamic analysis of the HDRB and LRB models under the input Northridge earthquake

7. Result and Discussion

The LRB undergoes a general static analysis procedure under a vertically concentrated load and subjected to cyclic lateral load, with the bottom end of the bearing fixed. A force-displacement curve is generated, and the results are compared with experimental and literature data. It was noted that the analyzed model closely aligns with both the manufacturer's specifications and previously analyzed results. Following optimization of the model for static analysis, the bearing is subsequently analyzed for dynamic behavior. The studies were performed [15][38-40] to evaluate the dynamic efficiency of the LRBs and HDRBs. The study conducted by Belbachir [11] shows a 54% reduction in acceleration for the HDRB+FVD isolated system compared to the fixed-base structure. The nonlinear dynamic analysis conducted on a fixed-base RC structure and three different base-isolated RC structures (employing HDRB, LRB, and elastomeric spring damper systems) provided the basis for a comparative analysis. This analysis includes the time history of base acceleration, base shear, base displacements, inter-storey drifts over time, and peak base shear values for each system [38]. Further, the study was performed to assessed dynamic responses of isolated structures, including crack distribution, acceleration, displacement, internal forces of bearings, and beam strains near failure. Sudden bearing failure, coupled with horizontal earthquakes, led to significant vertical deformation and impact. This affected adjacent and non-adjacent bearings, increasing the risk of overturning collapse. Vertical and low-frequency earthquake components notably influenced dynamic responses and damages, especially at bearing failure points [39]. In this study, the isolated bearing was simulated using ABAQUS CAE 2020 and subjected to time history records from the Imperial Valley, Managua, Loma Prieta, Northridge, and The Kocaeli events.

7.1 Validation of LRB and Analysis of HDRB

The response of the Lead Rubber Bearing (LRB) has been validated against experimental results from the manufacturer and numerical simulation analysis by Doudoumis using ADINA, as illustrated in Fig. 5. Additionally, a numerical simulation of the HDRB was conducted to analyze its force-displacement response as shown in Fig. 23. As the bearing undergoes cyclic loading, it exhibits a characteristic behavior in which the applied force increases progressively with displacement.

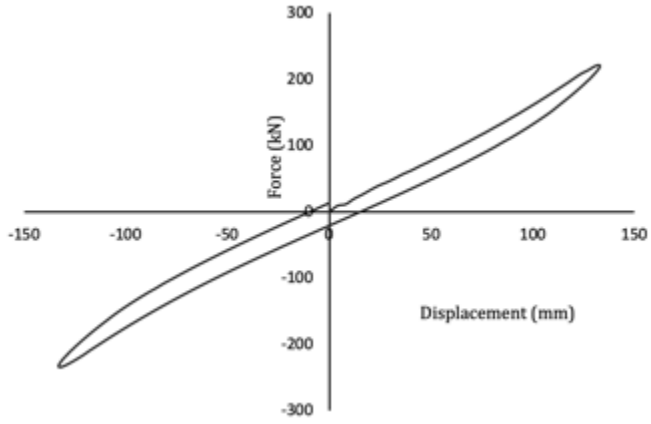

Fig. 23. Force-Displacement curve of the HDRB subject to horizontal cyclic loading

This is accompanied by a gradual stiffening of the bearing structure. Consequently, the displacement of the bearing is met with resistance, resulting in a nonlinear response where the force needed to induce further displacement increases gradually. This behavior is a

result of the high damping features of the rubber material within the bearing, which effectively dissipates energy and attenuates vibrations, contributing to the overall stability and performance of the bearing system. The analysis of HDRB and LRB revealed that the lead core in the LRB substantially enhances its performance. The static analysis showed good agreement between the analytical results and the experimental data, validating the precision of the models. These findings confirm the suitability of the numerical models for further dynamic analyses. Moreover, it highlights the efficacy of both LRBs and HDRBs in fortifying structures against seismic forces, emphasizing their role in bolstering structural resilience.

7.2 Acceleration Response

The results, based on accelerations at the top loading plate of the bearing, indicate that the isolation system was effectively activated during seismic events, ensuring the decoupling of motion between the superstructure and the foundations. Numerical analysis shows that the lead rubber bearing achieved a higher reduction in response compared to the HDRB. Specifically, the reduced acceleration responses in percentage are shown in Table 4 and the acceleration response in terms of 'g' for input, HDRB and LRB are shown in Fig. 24.

Table 4. Shows the acceleration response reduction for HDRB and LRB for input earthquake records

S.No.	Earthquake Records	HDRB response	LRB response
1.	The Kocaeli	48.42%	68.42%
2.	Imperial Valley	24.47%	57.24%
3.	Managua	48.35%	60.39%
4.	Loma Prieta	51.42%	62.05%
5.	Northridge	61.80%	68.41%

A notable decrease in the acceleration response at the top of the bearing was observed. This phenomenon indicates the effective dissipation of energy within the bearings, leading to reduced transmission of forces and vibrations to the superstructure. Such behavior is a key characteristic of these bearings, highlighting their ability to absorb and dissipate seismic energy, thereby safeguarding the structure against excessive vibrations.

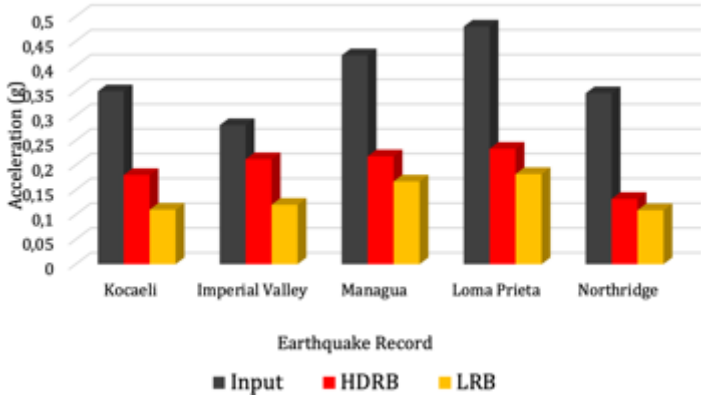

Fig. 24. Maximum acceleration at the top of the bearing with different input of the Time History earthquakes

7.3 Displacement Response

The displacement response at the top of the bearing is crucial for understanding structural behavior under seismic loading. It reveals how effectively bearings accommodate deformations and isolate the superstructure. A minimal or decreasing displacement indicates efficient energy dissipation and structural flexibility, reducing transmitted seismic forces. This highlights LRBs and HDRBs' ability to enhance seismic capacity by mitigating ground motion impact and preventing excessive deformations.

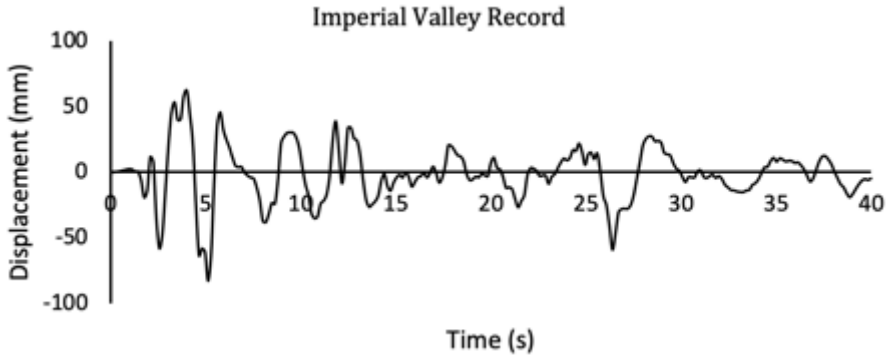

Fig. 25. The displacement response of the lead rubber bearing for time history function Imperial Valley

To prevent the overturning of isolators, it is crucial to restrict the horizontal displacement of the isolator. As per Chinese Code for the Seismic Design of Buildings, the maximum horizontal displacement of a rubber bearing during a ground motion should not exceed 0.55 times its effective diameter [41]. The displacement responses of the LRB for the Imperial Valley earthquake and the HDRB for the Managua earthquake, as illustrated in the respective Fig. 25 and Fig. 26, are provided. However, these responses, being at the top of the bearing, may not entirely reflect the actual behavior as it would occur within a complete building-bearings system.

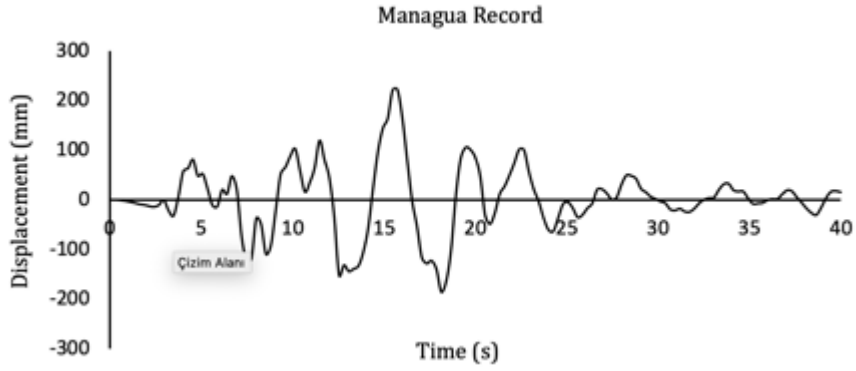

Fig. 26. The displacement response of the high damping rubber bearing for time history function Managua

8. Conclusion

In summary, the study comprehensively validated two types of isolators, LRBs and HDRBs, through a meticulous process involving static and dynamic analyses using 3D Finite Element (FE) models in Abaqus. The dynamic analysis revealed promising results, particularly in terms of acceleration and displacement responses. The bearings exhibited efficient energy dissipation, leading to reduced transmitted forces and vibrations to the superstructure. Furthermore, they demonstrated the capacity to withstand significant deformations, effectively protecting the superstructure from ground motion. These findings, presented in terms of the acceleration reduction within the bearing, highlight the effectiveness of LRBs and HDRBs in enhancing the seismic resilience of structures. This suggests their potential to mitigate ground motion impacts and prevent excessive structural deformations.

The hysteresis curves of HDRB show a smaller area compared to LRBs, indicating an unexpected lower energy dissipation capacity under similar shear deformation conditions. The horizontal shear performances of both types of bearings are illustrated in the force-displacement curve as shown in Fig. 4 for LRB and Fig. 21 for HDRB, indicating that the HDRB has a lower horizontal stiffness than the LRB under equivalent vertical loading and shear strain. This implies that, with an equal total rubber thickness, the steel plates in the HDRB exert less constraint force on the rubbers compared to the lead core in the LRB. The presence of the lead core enhances the energy dissipation capacity of the LRB.This study validates that both isolators significantly diminish the destructive effects of earthquakes, with LRBs showing superior performance over HDRBs. The maximum reductions in response are 68.42% for the Kocaeli earthquake in the case of LRBs and 61.80% for the Northridge earthquake in the case of HDRBs. The reduction in acceleration response at the top of the bearing is indicative of the bearings' effectiveness in mitigating the impact of seismic forces on the structure. This emphasizes their pivotal role in enhancing the collective seismic performance and safety of the structure.

In influence of near field ground motion excitation, the peak displacement for LRB under the Imperial Valley ground motion is 62.577mm, while for HDRB under the Managua earthquake record, it is 221.052mm.

Finite element micromodels provide detailed insights into the stress, strain, and strength characteristics of LRBs and HDRBs, aiding in the understanding of their mechanical behavior and facilitating improvements in their design. The inclusion of a lead core in LRBs alters stress and strain distribution, highlighting the necessity of micromodels for their study. It is essential to validate basic assumptions regarding material properties and fabrication details to ensure the accuracy of the analysis.

Dynamic analysis of HDRBs and LRBs in Abaqus is limited by the accuracy of material models for dynamic loading, large deformations, and high loading rates. Contact modeling, crucial for HDRBs and LRBs, can be challenging to accurately represent in Abaqus, impacting overall performance assessment. Additionally, results may be affected by material and interaction properties of the models, with dynamic analyses being computationally time consuming for complex models.

This research addresses the gap in the literature by focusing specifically on LRBs and HDRBs, applying ABAQUS software package for numerical simulations and finite element micro analysis. The results include a comparative analysis of the reduction in input earthquake forces, laying the foundation for future research in this field.

Future research in the analysis of HDRBs and LRBs using Abaqus should emphasize the development of more accurate material models, enhancements in contact algorithms, and

the refinement of dynamic loading simulations. Incorporating viscoelastic properties alongside other hyperelastic material models could be simulated numerically to identify the most optimized and improve models with enhanced precision and accuracy. It is crucial to conduct comprehensive experimental studies and parametric analyses to validate results and gain insights into the impact of various design parameters.

References

[1] Khan BL, Azeem M, Usman M, Farooq SH, Hanif A, Fawad M. Effect of near and far field earthquakes on performance of various base isolation systems. Procedia Struct Integr. 2019;18:108–18.

[2] Işık E. Comparative investigation of seismic and structural parameters of earthquakes (M ≥ 6) after 1900 in Turkey. Arab J Geosci. 2022;15(10):971.

[3] Bilgin H, Hadzima-Nyarko M, Isik E, Ozmen HB, Harirchian E. A comparative study on the seismic provisions of different codes for RC buildings. Struct Eng Mech. 2022;83(2):195–206.

[4] Akar F, Işık E, Avcil F, Büyüksaraç A, Arkan E, İzol R. Geotechnical and Structural Damages Caused by the 2023 Kahramanmaraş Earthquakes in Gölbaşı (Adıyaman). Appl Sci. 2024;14(5):2165.

[5] Bilgin H. Effects of near-fault and far-fault ground motions on nonlinear dynamic response and seismic damage of masonry structures. Eng Struct. 2024;300(November 2023):117200. https://doi.org/10.1016/j.engstruct.2023.117200

[6] Standards ASCE/SEI 7-16. Minimum Design Loads and Associated Criteria for Buildings and Other Structures. ASCE Standard.

[7] Sheikh H, Van Engelen NC, Ruparathna R. A review of base isolation systems with adaptive characteristics. Structures. 2022;38(March):1542–55. https://doi.org/10.1016/j.istruc.2022.02.067

[8] Weisman J, Warn GP, Asce AM. Stability of Elastomeric and Lead-Rubber Seismic Isolation Bearings. J Struct Eng. 2012;138(2):215–23.

[9] Zhang C, Ali A. The advancement of seismic isolation and energy dissipation mechanisms based on friction. Soil Dyn Earthq Eng. 2021;146(11):106746. https://doi.org/10.1016/j.soildyn.2021.106746

[10] Patel D, Mourya VK, Pandey G, Kumar R. Advancements in base isolation for seismic mitigation : Perspectives on elastomeric and lead rubber bearings. Res Eng Struct Mater. 2024;1–33 http://dx.doi.org/10.17515/resm2024.15ma0927rv

[11] Belbachir A, Benanane A, Ouazir A, Harrat ZR, Hadzima-Nyarko M, Radu D, et al. Enhancing the Seismic Response of Residential RC Buildings with an Innovative Base Isolation Technique. Sustain. 2023;15(15).

[12] Markou AA, Manolis GD. Mechanical models for shear behavior in high damping rubber bearings. Soil Dyn Earthq Eng. 2016;90:221–6. http://dx.doi.org/10.1016/j.soildyn.2016.08.035

[13] Yoshida J, Abe M, Fujino Y. Constitutive Model of High Damping Rubber Materials. Doboku Gakkai Ronbunshu. 2002;2002(710):209–24.

[14] Clemente P, Bongiovanni G, Buffarini G, Saitta F, Gabriella M, Scafati F. Effectiveness of HDRB isolation systems under low energy earthquakes. Soil Dyn Earthq Eng. 2019;118(December 2018):207–20. https://doi.org/10.1016/j.soildyn.2018.12.018

[15] Alhan C, Gazi H, Kurtulu H. Significance of stiffening of high damping rubber bearings on the response of base-isolated buildings under near-fault earthquakes. Mech Syst Signal Process. 2016;

[16] Bandyopadhyay S, Parulekar YM, Sengupta A, Chattopadhyay J. Structure soil structure interaction of conventional and base-isolated building subjected to real earthquake. Structures. 2021;32(March):474–93.

https://doi.org/10.1016/j.istruc.2021.03.069
[17] Pandey G, Patel D, Mourya VK. A Review on Soil - Foundation - Interaction Models. J Rehabil Civ Eng. 2023;3(11):158–79. https://doi.org/10.22075/JRCE.2022.25247.1570
[18] Pandey G, Mourya VK, Patel D, Kumar R. Load sharing behaviour in piled-raft foundations over sand and clay : An experimental investigation. Res Eng Struct Mater. 2023;1–26. http://dx.doi.org/10.17515/resm2023.41me0714rs
[19] Mourya VK, Pandey G, Patel D, Kumar R. Approaches considering non-linearity in soil-foundation-interaction: A State of the Art Review. Res Eng Struct Mater. 2023;9(3):989–1013. http://dx.doi.org/10.17515/resm2023.646me0117
[20] Ozdemir G, Avsar O, Bayhan B. Change in response of bridges isolated with LRBs due to lead core heating. Soil Dyn Earthq Eng. 2011;31(7):921–9. http://dx.doi.org/10.1016/j.soildyn.2011.01.012
[21] Ozdemir G, Dicleli M. Effect of lead core heating on the seismic performance of bridges isolated with LRB in near-fault zones. Earthq Eng Struct Dyn. 2012;41(14):1989–2007.
[22] Arguc S, Avsar O, Ozdemir G. Effects of Lead Core Heating on the Superstructure Response of Isolated Buildings. J Struct Eng. 2017;143(10):04017145.
[23] Hu GJ, Ye K, Tang ZY. Design and analysis of LRB base-isolated building structure for multilevel performance targets. Structures. 2023;57(July):105236. https://doi.org/10.1016/j.istruc.2023.105236
[24] Basshofi Habieb A, Tavio T, Milani G, Wijaya U. 3D-Finite element modeling of lead rubber bearing using high damping material. MATEC Web Conf. 2019;276:01013.
[25] Behzad Talaeitaba S, Safaie M, Zamani R. Development and application of a new base isolation system in low-rise buildings. Structures. 2021;34(July):1684–709. https://doi.org/10.1016/j.istruc.2021.07.077
[26] Pourmasoud M, Park ARL, Hajirasouliha I, Lim J, Behzadi A. Validation of a New Equation to Estimate the Yield Strength of Lead Rubber Bearings. Procedia Struct Integr. 2022;44(2022):590–7. https://doi.org/10.1016/j.prostr.2023.01.077
[27] Rahgozar A, Estekanchi HE, Mirfarhadi SA. On optimal lead rubber base-isolation design for steel moment frames using value-based seismic design approach. Soil Dyn Earthq Eng. 2023;164(July 2022):107520. https://doi.org/10.1016/j.soildyn.2022.107520
[28] Saiful Islam ABM, Jameel M, Jummat MZ. Study on optimal isolation system and dynamic structural responses in multi-storey buildings. Int J Phys Sci. 2011;6(9):2219–28.
[29] Ounis HM, Ounis A, Djedoui N. A new approach for base isolation design in building codes. Asian J Civ Eng. 2019;20(6):901–9. https://doi.org/10.1007/s42107-019-00153-x
[30] Güneş N. Effects of near-fault pulse-like ground motions on seismically isolated buildings. J Build Eng. 2022;52(April):1–17.
[31] Güneş N, Ulucan ZÇ. Nonlinear dynamic response of a tall building to near-fault pulse-like ground motions. Bull Earthq Eng. 2019;17(6):2989–3013. https://doi.org/10.1007/s10518-019-00570-y
[32] Güneş N. Risk-targeted design of seismically isolated buildings. J Build Eng. 2022;46(August 2021):1–16.
[33] Kelly JM. Analysis of fiber-reinforced elastomeric isolators. J Seism Earthq Eng. 1999;2(1):19–34.
[34] Imbimbo M, De Luca A. F.E. stress analysis of rubber bearings under axial loads. Comput Struct. 1998;68(1–3):31–9.
[35] Doudoumis IN, Gravalas F. Analytical Modeling of Elastomeric Lead-Rubber Bearings with the use of Finite Element Micromodels. In: 5th GRACM International Congress on Computational Mechanics. 2005.

[36] Evaluation findings for skellerup base isolation elastomeric bearings. Technical evaluation report, (CERF report: HITEC 98-12), prepared by the Highway Innovative Technology Evaluation Center. 1998;
[37] PEER. User's manual for the peer ground motion database application. Pacific Earthq Eng Res Center Univ California, Berkeley. 2011;
[38] Cancellara D, Angelis F De. Nonlinear dynamic analysis for multi-storey RC structures with hybrid base isolation systems in presence of bi-directional ground motions. Compos Struct. 2016;154:464–92. http://dx.doi.org/10.1016/j.compstruct.2016.07.030
[39] Han B, Du Y, Hong N, Li H, Shi C. Shaking table test study on dynamic performance of a base-isolated frame structure under an isolation bearing removal scenario. Structures. 2023;48(January):1141–56.
[40] Tagliafierro B, Montuori R, Castellano MG. Shake table testing and numerical modelling of a steel pallet racking structure with a seismic isolation system. Thin-Walled Struct. 2021;164(October):107924. https://doi.org/10.1016/j.tws.2021.107924
[41] Zhang R, Wu M, Lu W, Li X, Lu X. Seismic retrofitting of a historic building by using an isolation system with a weak restoring force. Soil Dyn Earthq Eng. 2021;148(January):106836. https://doi.org/10.1016/j.soildyn.2021.106836